Quantum vortices, travelling coherent structures and superfluid turbulence

Natalia G. Berloff

Abstract. The Gross-Pitaevskii equation and its modifications are used to elucidate different aspects of superfluid behaviour: motion of vortices, travelling waves, interactions with normal fluid and superfluid turbulence. Different mechanisms of formation of travelling coherent structures are considered. They are formed when a critical velocity is exceeded in the flow. They can appear as a result of instabilities or energy transfer among waves. They are formed together with the formation of condensate, but the interactions with normal fluid (non-condensed particles) lead to their dissipation.

1. Introduction

Superfluidity is the ability to flow through narrow channels without friction; this phenomenon is characterised by the existence of quantised vortices with the quantum of circulation $\kappa = h/m$, where m is the mass of a boson. Superfluidity is closely related to the Bose-Einstein condensation (BEC) – the state of matter in which a large percentage of bosons collapse into their lowest quantum state, allowing quantum effects to be observed on a macroscopic scale. This phenomenon has been first realised experimentally in dilute atomic gases in 1995 and since that time many more superfluid system has been experimentally obtained: Fermi gases, exciton-polariton condensates, multi-component BEC, etc. The link between superfluidity and BEC is in the existence of the classical field ψ (*order parameter, wave function*) associated with the macroscopic component of the field operator. The order parameter ψ is the complex function (or several complex functions for multi-component condensates, or 3x3 matrix of complex functions for ^{3}He) where, quantum mechanically, density, ρ_s, is the square of the amplitude and velocity, $\mathbf{v}_s$ is proportional to the gradient of the phase, S:

$$\psi = \sqrt{\rho_s}\exp[\mathrm{i}S], \qquad \mathbf{v}_s = \frac{\hbar}{m}\nabla S. \tag{1.1}$$

The existence of quantised vortices immediately follows from this representation. If we draw a closed contour C in a singly-connected superfluid system described by ψ, then the phase S of ψ can only change by a multiple of 2π for ψ to remain single valued as we move around this contour. If the phase S does indeed changes by, say, 2π, then there has to be at least one point (in 2D) or a line (in 3D) inside C where S takes any value between 0 and 2π. To prevent such phase singularity, the density, ρ_s, has to vanish at this point (line). These points or lines are therefore quantised vortices with the unit of circulation $\int_C \mathbf{v}_s \cdot d\mathbf{l} = 2\pi\hbar/m = h/m$, as stated above.

The first successful macroscopic theory for the motion of superfluid helium (HeII) was that of Landau [**1**], in which the fluid is modelled as an interacting mixture of superfluid of density ρ_s moving with velocity $\mathbf{v}_s$ and a normal fluid of density ρ_n moving with velocity $\mathbf{v}_n$, representing the phonons and

Key words and phrases. Superfluid, Gross-Pitaevskii, vortices, turbulence.
The author was supported by EPSRC-UK.

rotons that ride on the superfluid. As the temperature T tends to absolute zero, $\rho_n \to 0$ and $\rho_s \to \rho$ (the total density of the mixture). As $T \to T_\lambda$, the temperature of the phase transition to helium I, $\rho_s \to 0$ and $\rho_n \to \rho$. The range $T < 0.6$K is often defined to be the 'low temperature regime', while 0.6K $< T < T_\lambda$ is the 'high temperature regime', in which most experiments on superfluid turbulence have been performed, and in which the normal fluid determined by the turbulence taking place in the normal fluid. This is confirmed by the success of theories of superfluid turbulence, such as that of Barenghi et al. [**2**], [**3**], in which the superfluid vorticity is largely tied to that of the normal fluid. In contrast, in the low temperature range ($T \leq 0.6°K$), where ρ_n is smaller than ρ_s, we may expect turbulence in the superfluid largely to determine turbulence in the normal fluid, rather than the reverse.

In the low temperature regime, $\rho_n/\rho_s \ll 1$, and the normal fluid plays a relatively minor role. Even though the superfluid is inviscid, there are significant differences between classical turbulence at large Reynolds number and superfluid turbulence. The most significant is that vorticity is continuously distributed in a classical (Navier-Stokes) fluid, but is quantised in a superfluid in units of κ. Turbulence in the superfluid therefore resembles a tangle of vortex filaments, whose dynamics differs from that of the chaotic but continuous vorticity of classical turbulence; see, for example, [**4**].

1.1. The first approach: HVBK theory. The Landau [**1**] theory of superfluidity pre-dated the discovery of quantised vortex lines and therefore omitted significant dynamical effects. This was remedied, in the limit in which the mean spacing b between the vortex lines is small compared with any other length scale L of interest, by HVBK theory, so named after Hall and Vinen [**5**] who first set up such a theory, and Bekharevich and Khalatnikov [**6**] who generalised it; see also Hills and Roberts [**7**]. In this limit ($b \ll L$), the superfluid vorticity is treated as a continuum, but the discrete nature of the vorticity gives rise to an extra force $\mathbf{T}$ on the superfluid component, arising from the tension in the vortex lines; this term is absent from the classical Euler equation of motion for an inviscid fluid. The vortex lines also create a force $\mathbf{F}$ of mutual friction between superfluid and normal fluid that is additional to the mutual friction included by Landau in his equations, and represents the effects of collisions of the quasiparticles with the vortex cores. HVBK theory has scored a number of successes. It has given results [**8**] in quantitative agreement with experiments on the instability of Taylor-Couette flow in HeII [**9**]. HVBK theory provides the first of three principal ways of studying superfluid turbulence.

1.2. The second approach; classical theory of vortex filaments. The second approach recognises that HVBK theory presupposes a high density of pre-existing superfluid vortex lines, and is incapable of describing processes that create or destroy those lines. For example, the assumption $b \ll L$ implies that the superfluid vorticity, $\boldsymbol{\omega}_s$, varies slowly with position $\mathbf{x}$. This excludes situations favourable to the reconnection of lines, such as when oppositely-directed vortex lines are brought by the flow into juxtaposition. To understand the creation and destruction of lines, it is necessary to study situations in which b is *not* small compared with L, and in which vortex lines are treated as discrete entities. The term "superfluid turbulence" is often used synonymously for the "evolution of superfluid vortices." On the scale much larger than the vortex core radius ($a \approx 10^{-8}cm$) the motion of superfluid vortices is commonly described by the classical theory of vortex filaments. If superfluid vortices are modelled as filaments of zero cross-section with $\delta-$function vorticity, the kinematic statements $\boldsymbol{\nabla}\cdot\mathbf{v} = 0, \boldsymbol{\nabla}\times\mathbf{v} = \boldsymbol{\omega}$ imply a line integral along the filaments, $\mathbf{s} = \mathbf{s}(\xi)$, where ξ is arc length:

$$\mathbf{v}(\mathbf{x}) = \frac{\kappa}{4\pi}\int \frac{\mathbf{s}'\times(\mathbf{x}-\mathbf{s})d\xi}{|\mathbf{x}-\mathbf{s}|^3}, \tag{1.2}$$

in which $\mathbf{s}'(\xi) = d\mathbf{s}/d\xi$ is the unit tangent vector. The integral (1.2) known as the Biot-Savart Law (BSL) diverges however in the limit $\mathbf{x} \to \mathbf{s}_1$, where $\mathbf{s}_1 = \mathbf{s}(\xi_1)$ is any point on a filament; the nature of the divergence is spelled out in detail in §2.3 of [**10**]. To salvage (1.2) the 'cut-off method' was introduced. When computing the velocity $\mathbf{v}(\mathbf{s}_1)$ of the filament at $\mathbf{x} = \mathbf{s}_1$, the segment $|\xi - \xi_1| < \delta$, where $\delta = \mathrm{O}(a)$,

is simply deleted from (1.2). The best choice of δ has been determined when the radius of curvature, $R(\xi_1)$, at $\mathbf{s}_1$ is large compared with a. When $R \ll L$, the motion of the vortex at $\mathbf{s}_1$ is decided mainly by the distribution of the vorticity $\boldsymbol{\omega}(\mathbf{s})$ in the vicinity of $\mathbf{s}_1$ and, to a first approximation,

$$\mathbf{v}(\mathbf{s}_1) = (\kappa/4\pi)(\mathbf{s}_1' \times \mathbf{s}_1'') \ln(\ell/a), \tag{1.3}$$

where $\ell = \mathrm{O}(R)$. This is known as the 'local induction approximation' (LIA), and is the most convenient, but also the crudest, way of determining the motion of vortex lines. It is especially dubious when (as is often the case) the conditions $a \ll R \ll L$ are not met.

It is clear that the application of classical theory is not free of difficulty. Moreover, two mechanisms very relevant to superfluid turbulence are ignored. It has recently been shown [**11**] that emission of sound by a vortex tangle is very significant in superfluid turbulence. This process is completely removed by the main assumption of classical vortex theory: $\boldsymbol{\nabla} \cdot \mathbf{v}_s = 0$. The dynamics of vortex filaments in a compressible fluid is not as well understood as that for the incompressible case. Secondly, the processes of severance and coalescence of vortex lines are centrally important for the study of superfluid turbulence, but these are explicitly forbidden by the Kelvin-Helmholtz theorem, according to which vortex lines are frozen to an Euler fluid and cannot change their topology. In a normal fluid, the processes have been successfully simulated numerically by restoring viscosity to the fluid. This step is disallowed in a superfluid, and the only way to defeat the theorem is through *ad hoc* procedures. For example, it has been supposed that, whenever one vortex filament comes within a distance Δ of order a of another filament, reconnection will always occur, and that otherwise reconnection will not happen. A precise way of determining Δ is not known, but its value can clearly greatly affect the reconnection rate in a vortex tangle. Moreover, the angle at which the vortex filaments approach one another is undoubtedly an important factor in determining whether they reconnect or not; a clear set of *reconnection rules* is lacking.

1.3. The third approach; GP theory. We now move to the third approach, a theory that gives superfluid vortex lines their own unique core structure. At the same time, it provides a mechanism for the severing and coalescence of vortex lines, and includes sound propagation, so that the emission of sound from a vortex tangle can be evaluated. In short, while having the same objectives as the second approach, it evades all of its difficulties (although it has a few difficulties of its own).

In the Hartree approximation, the imperfect Bose condensate is governed by the GP equation [**12**]. In terms of the single-particle wavefunction $\psi(\mathbf{x}, t)$ for N bosons, the time-dependent self-consistent field equation is

$$\mathrm{i}\hbar\psi_t(\mathbf{x}, t) = -(\hbar^2/2m)\nabla^2\psi(\mathbf{x}, t) + \psi(\mathbf{x}, t) \int |\psi(\mathbf{x}', t)|^2 V(|\mathbf{x} - \mathbf{x}'|)\, d^3x' - E_v\psi(\mathbf{x}, t), \tag{1.4}$$

where $V(|\mathbf{x} - \mathbf{x}'|)$ is the potential of the two-body interactions between bosons, and E_v is the chemical potential which we explicitly introduce into the system. The normalisation condition is $\int |\psi|^2\, d^3x = N$. For a weakly interacting Bose gas, (1.4) is simplified by replacing $V(|\mathbf{x} - \mathbf{x}'|)$ with a $\delta-$function repulsive potential of strength V_0. This does not qualitatively alter the nature of the results since the characteristic length of the weakly interacting Bose gas is larger than the range of the force. Equation (1.4) for such a potential is

$$\mathrm{i}\hbar\psi_t(\mathbf{x}, t) = -(\hbar^2/2m)\nabla^2\psi + V_0|\psi|^2\psi - E_v\psi. \tag{1.5}$$

Equations (1.4)-(1.5) define Hamiltonian systems, the following integrals being conserved: mass

$$M = m \int |\psi|^2\, d\mathbf{x}, \tag{1.6}$$

momentum density

$$\mathbf{p} = \frac{\hbar}{2\mathrm{i}} \int [\psi^* \nabla\psi - \psi \nabla\psi^*]\, d\mathbf{x}, \tag{1.7}$$

and energy; in the case of (1.5) this is expressed by

$$E = \frac{\hbar^2}{2m} \int |\nabla\psi|^2\, d\mathbf{x} + \frac{V_0}{2} \int |\psi|^4\, d\mathbf{x}. \tag{1.8}$$

It is usually convenient to model phenomena in an infinite domain in which, prior to the onset of a disturbance, $\psi = \psi_\infty$ everywhere, where, by (1.5)

$$\psi_\infty = (E_v/V_0)^{1/2}. \tag{1.9}$$

We then modify (1.7)-(1.8) to forms measuring departures from this uniform state

$$\mathbf{p} = \frac{\hbar}{2\mathrm{i}} \int [(\psi^* - \psi_\infty)\nabla\psi - (\psi - \psi_\infty)\nabla\psi^*]\, d\mathbf{x}, \tag{1.10}$$

$$E = \frac{\hbar^2}{2m} \int |\nabla\psi|^2\, d\mathbf{x} + \frac{V_0}{2} \int (|\psi|^2 - \psi_\infty^2)^2\, d\mathbf{x}. \tag{1.11}$$

The Madelung transformation relates the wave function, $\psi = R \exp \mathrm{i}S$, to classical hydrodynamical variables. The mass density ρ, mass flux $\mathbf{j}$ and velocity potential ϕ, are $\rho = mR^2, \mathbf{j} = \rho\mathbf{v} = \rho\boldsymbol{\nabla}\phi, \phi = (\hbar/m)S$. The real and imaginary parts of (1.5) then give a continuity equation and an integrated form of the momentum equation:

$$\rho_t + \boldsymbol{\nabla}\cdot(\rho\mathbf{v}) = 0, \tag{1.12}$$

$$\frac{\partial\phi}{\partial t} + \frac{1}{2}v^2 + c^2\left(\frac{\rho}{\rho_\infty} - 1\right) = c^2a^2\frac{\nabla^2\rho^{1/2}}{\rho^{1/2}}, \tag{1.13}$$

where $\rho_\infty = mE_v/V_0$ is the density at infinity (the density of the fluid when stagnant), c is the speed of sound $c = \sqrt{E_v/m} = (V_0/m^2)^{1/2}\rho_\infty^{1/2}$ and $a = \kappa/2\sqrt{\pi}c$ is the so-called 'healing length'. The healing length is the characteristic length on which fluid heals itself when locally perturbed. It also fixes the vortex core size, see Sec. 1.2. The final term in (1.13) is sometimes called the 'quantum pressure'. It may be particularly noticed that, while the fluid flows irrotationally, it is not incompressible. According to (1.13) and temporarily ignoring its right-hand side, the pressure P is proportional to ρ^2: $P = (c^2/2\rho_\infty)\rho^2$. Motion in the fluid is accompanied by sound waves.

The elementary excitations (small amplitude harmonic modes) above the ground state (the lowest energy state for a given number of particles) $\psi_0 = \sqrt{\rho_0/m} = \sqrt{E_v/V_0}$ are found by inserting $\psi = \psi_0(\mathbf{x}) + \epsilon\psi_1(\mathbf{x}, t)$ into the GP equation (1.5) and linearising it to

$$i\hbar\psi_{1t} = -\frac{\hbar^2}{2m}\nabla^2\psi_1 + \frac{\rho_0 V_0}{m}(\psi_1 + \psi_1^*). \tag{1.14}$$

We look for plane wave modes: $\psi_1 = A\exp[i(\mathbf{k}\cdot\mathbf{x} - \omega t)] + B^*\exp[-i(\mathbf{k}\cdot\mathbf{x} - \omega t)]$, where A and B are complex constants. The existence of a non-trivial solution for A and B implies the dispersion relation (Bogoliubov law) as

$$\omega^2 = \frac{\rho_0 V_0}{m^2}k^2 + \left(\frac{\hbar k^2}{2m}\right)^2. \tag{1.15}$$

For small k (long wavelengths) the dispersion is sound-like $\omega \approx ck$. The corresponding quasiparticles are *phonons*. For large k (short wavelengths) the dispersion is particle-like $\omega \approx \hbar k^2/2m$.

A vortex filament is no more than a curve on which $\psi = 0$, and there is no reason why such curves should not intersect or divide. Using the hydrodynamical interpretation of (1.5), these processes

correspond to the coalescence or severance of vortex lines. There is no violation of the Kelvin-Helmholtz theorem, which does not apply to integration paths passing through zeros of ρ. In short, the GP equation provides a means of studying these important changes of topology of a vortex tangle without making any *ad hoc* assumptions, and while remaining within the framework of Hamiltonian dynamics, i.e., without introducing viscosity. There is also no need to appeal to the BSL or LIA approximations, which are in any case somewhat misleading, since the fluid is compressible.

In what follows we consider the GP equation and its modifications as models of superfluid turbulence paying a particular attention to vortices and travelling coherent structures that these equations exhibit. We shall often refer to dimensionless GP equation (1.5)

$$-2i\psi_t = \nabla^2\psi + (1 - |\psi|^2)\psi, \tag{1.16}$$

where time is measured in units of $ma^2/\hbar$ and distance in healing lengths a. The impulse (1.10) and energy (1.11) become

$$\mathbf{p} = \frac{1}{2i}\int \nabla\psi(\psi^* - 1) - \nabla\psi^*(\psi - 1)\, d\mathbf{x}, \tag{1.17}$$

measured in $\hbar/a$ and

$$E = \tfrac{1}{2}\int |\nabla\psi|^2 + \tfrac{1}{2}(1 - |\psi|^2)^2\, d\mathbf{x} \tag{1.18}$$

measured in $\hbar^2\rho_\infty/m^2$.

We discuss a single straight line vortex and the vortex motion on uniform and non-uniform backgrounds in Section II. We modify the GP equation to make it more applicable to superfluid helium in Section III. Travelling coherent structures that exist in the GP equation, the nonlocal GP equation and the coupled GP equations are subject of our study in Section IV. In Section V we consider mechanisms of the formation of these localised structures. We discuss how to introduce the normal component into superfluid in Section VI, where we also study the dissipation of a vortex ring at non-zero temperatures.

2. Vortices

A vortex line is defined by a zero of the wave function $\psi = 0$. In cylindrical coordinates (r, θ, z) the wave function of a straight-line vortex takes form

$$\psi = R(r)\exp[is\theta], \tag{2.1}$$

where s is an integer ("winding number", "topological charge"). Fluid rotates around the z-axis with tangential velocity

$$v = \frac{\hbar}{m}\nabla\theta = \frac{\hbar}{m}\frac{s}{r} \tag{2.2}$$

and the amplitude satisfies

$$-\frac{\hbar^2}{2m}\frac{1}{r}\frac{d}{dr}\left(r\frac{dR}{dr}\right) + \frac{\hbar^2 s^2}{2mr^2}R + V_0R^3 - E_vR = 0. \tag{2.3}$$

At large distances the density is unperturbed, so $R \to \psi_\infty$. We introduce the dimensionless function $R = \psi_\infty f(\eta)$, where the distance is measured in healing lengths $\eta = r/a$.

$$\frac{1}{\eta}\frac{d}{d\eta}\left(\eta\frac{df}{d\eta}\right) + \left(1 - \frac{s^2}{\eta^2}\right)f - f^3 = 0, \qquad f(\infty) = 1. \tag{2.4}$$

This equation was numerically integrated by Pitaevskii [**13**] and the solution is shown on Fig. 1 together with a Padé approximation [**14**].

FIGURE 1. The amplitude of a straight-line vortex for $s = 1$ as solution of Eq. (2.4). The leading order terms of the power series expansions at zero and infinity are shown next to the graph. A Padé approximation of the vortex amplitude $\eta/\sqrt{\eta^2+2}$ is shown by dashed (red) line.

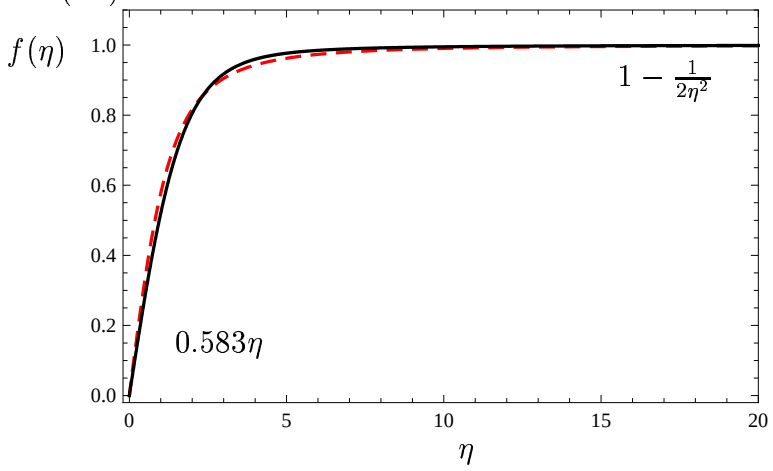

The simplest Padé approximation of the vortex amplitude that will be used to analyse vortex motion is in the form $f(\eta)^2 = \eta^2/(\eta^2+2)$ [**15**], so the wavefunction of a straight line vortex is approximated by

$$\frac{\psi}{\psi_\infty} = f(\eta)e^{i\theta} = (x+iy)/\sqrt{x^2+y^2+2}, \quad x = \eta\cos\theta, y = \eta\sin\theta. \tag{2.5}$$

The energy per unit length of the vortex line is

$$E_\ell = \frac{\kappa^2\rho_\infty}{4\pi}\left(\int_0^\infty \left[\frac{dR}{dr}\right]^2 r\,dr + \int_0^\infty \frac{R^2}{r}\,dr + \frac{1}{2}\int_0^\infty (1-R^2)^2 r\,dr\right). \tag{2.6}$$

The first term can be regarded as a "quantum energy", the second term is the classical vortex kinetic energy that diverges logarithmically unless a cut-off distance L is introduced; the third term in (2.6) represents the potential energy. The energy per unit length of the vortex is usually expressed in the form

$$E_\ell = \frac{\kappa^2\rho_\infty}{4\pi}\left(\ln\frac{L}{a} + L_0\right), \tag{2.7}$$

where the constant L_0 is called the "vortex core parameter" and was determined numerically by Pitaevskii [**13**] as $L_0 = 0.3809$.

Straight-line vortices can transmit energy along their length by Kelvin waves. These have been comprehensively analysed for incompressible Euler fluids; see for example Chapter 11 of Saffman [**10**]. They have been studied for compressible hollow core and the GP vortices by Roberts [**16**] who showed that in both situations, the waves may be bound or free, depending on their angular and axial wave numbers, m_θ and k. The free waves radiate energy acoustically to infinity, while the bound states do not. It is found that for the GP vortex one class of $m_\theta = 1$ modes, called 'slow modes' because of their low frequency, consists of bound states for all k. The slow $m_\theta = 2$ modes are also bound when k is sufficiently large, but are free for small k.

2.1. Vortex motion on uniform backgrounds. Here we consider N_v vortices in (x, y)-plane that are separated by distances far exceeding the healing length a and satisfying Eq. (1.16).

we introduce a small parameter $\epsilon = a/L$, where L is an average inter-vortex distance and scales $\nabla \to \epsilon\nabla, \partial_t \to \epsilon^2\partial_t$ and get to the leading order from Eq.(1.16)

$$\rho = 1 - O(\epsilon^2), \qquad \nabla^2 S = 0. \tag{2.8}$$

This shows that the vortex motion is according to classical inviscid irrotational (except at the vortex positions $\mathbf{x} = \mathbf{x}_i$) incompressible flow dynamics. The velocity potential for a point vortex at origin, with the winding number s, is $s\theta$, so

$$\mathbf{v} = s\nabla\theta = s\frac{\mathbf{e}_z \times \mathbf{x}}{|\mathbf{x}|^2} = sJ\frac{\mathbf{x}}{|\mathbf{x}|^2},$$

where J denotes rotation through $\pi/2$.

Laplace's equation (2.8) is linear, so we can linearly superpose a finite number N_v of point vortices with different strengths and positions $\mathbf{x}_i$ $(i = 1, ...N_v)$, thus

$$\mathbf{v} = \sum_i s_i \frac{\mathbf{e}_z \times (\mathbf{x} - \mathbf{x}_i)}{|\mathbf{x} - \mathbf{x}_i|^2}.$$

Classical point vortices move as material points so each vortex is moved by the velocity field due to all the other vortices. The dynamical system of vortex motion takes the form

$$\dot{\mathbf{x}}_i(t) = \sum_{j \neq i} s_j \frac{\mathbf{e}_z \times (\mathbf{x}_i - \mathbf{x}_j)}{|\mathbf{x}_i - \mathbf{x}_j|^2} \ (i = 1, ...N_v) \ .$$

Remarkably, the equations of vortex motion have a Hamiltonian structure:

$$s_i\dot{\mathbf{x}}_i(t) = J\frac{\partial H}{\partial \mathbf{x}_i}; \qquad H = \frac{1}{2}\sum_j \sum_{j \neq i} s_i s_j \ln|\mathbf{x}_i - \mathbf{x}_j|.$$

In general it is quite challenging to understand vortex motion in condensates as vortices move on essentially nonuniform backgrounds, interacting with sound and emitting sound. Next we consider motion of a vortex line near a solid boundary and show that for a vortex parallel to the wall, the motion is essentially equivalent to that generated by an image vortex, but the depleted surface layer induces an effective shift in the position of the image compared to the case of a vortex pair in an otherwise uniform flow.

2.2. Vortex motion near the boundary. Here we consider the problem of vortex motion in an asymptotically homogeneous condensate in the presence of a solid wall where the wave function of the condensate vanishes. Again, the geometry is two dimensional, with the vortex aligned along the z axis, parallel to the surface of the wall. The dynamics of the time-dependent condensate in the presence of the solid wall at $y = 0$ is described by the GP equation (1.16) subject to the boundary condition

$$\psi(x, y = 0, t) = 0, \quad |x| < \infty. \tag{2.9}$$

In the absence of vortices, the exact solution of (1.4) for the stationary state of the semi-infinite condensate is

$$f(y) = \tanh(y/\sqrt{2}). \tag{2.10}$$

In classical inviscid fluid dynamics with constant mass density ρ, the relevant kinematic boundary condition at a solid wall with normal vector $\mathbf{n}$ is

$$\rho\,\mathbf{u} \cdot \mathbf{n} = 0, \tag{2.11}$$

where ρ is the local density of the fluid and $\mathbf{u}$ is the velocity of the fluid. The corresponding problem of a vortex moving parallel to the wall is solved by placing one or more image vortices in such a way that condition (2.11) is identically satisfied.

For the dynamics described by the GP equation (1.4), the density $\rho \propto |\psi|^2$ is no longer constant, but rather vanishes at the surface of the wall. Thus condition (2.11) is automatically satisfied, and all components of $\mathbf{u}$ can in principle remain finite on the boundary. Therefore, it may seem that image vortices are irrelevant in the case of the GP equation, so that the vortex should remain stationary away from the boundary (where the fluid density is constant apart from exponentially small corrections). It was shown in [**17**] that this is not true. In fact, the vortex moves parallel to the boundary, and it moves faster than a corresponding pair of vortices of opposite circulation in a uniform condensate in the absence of the depletion caused by the boundary.

The asymptotics of the vortex velocity was obtained using the Hamiltonian group relation

$$U = \frac{\partial E}{\partial p}, \tag{2.12}$$

which is satisfied by classical as well as the GP vortex pairs and vortex rings moving on homogeneous backgrounds [**18**]. The Hamiltonian relation (2.12) is derived by considering the variation $\psi \to \psi + \delta\psi$ in (1.17) and (1.18) that results in

$$\delta p = \mathrm{i} \int \delta\psi \frac{\partial \psi^*}{\partial x} - \delta\psi^* \frac{\partial \psi}{\partial x}\, dxdy \tag{2.13}$$

and

$$\delta E = \tfrac{1}{2} \int \delta\psi^* \left[-\nabla^2\psi + \psi\left(|\psi|^2 - 1\right)\right] + \delta\psi \left[-\nabla^2\psi^* + \psi^*\left(|\psi|^2 - 1\right)\right] dxdy\,, \tag{2.14}$$

provided $\delta\psi \to 0$ as $y \to \infty$. It follows that $\delta E = U\delta p$ and thus the Hamiltonian group relation of the energy and momentum taken along the sequence of solitary-waves that satisfy Eq. (1.16) with $\partial_t \to -U\partial_x$. We compare the motion of a pair of vortices of opposite circulation distance $2y_0$ away from each other with the approximate form of the wavefunction $\psi_1 = \psi_v(y_0)\psi_v^*(-y_0)$ where $\psi_v(y_0) = \psi(x, y - y_0)$ and ψ is given by Eq. (2.5) with the motion of a vortex distance $y_0 + l$ away from the solid wall, approximated by $\psi_2 = \tanh(y/\sqrt{2})\psi_v(y_0 + l)\psi_v^*(-y_0 - l)$. If the pair and a vortex move with the same (classical) velocity $1/2y_0$, then

$$l = y_0 - \frac{1}{2}\frac{\partial p/\partial y_0}{\partial E/\partial y_0}, \tag{2.15}$$

where E and p are energy and impulse of a vortex next to a solid wall (given by Eqs.(1.18)–(1.17) but with ψ_∞ replaced by the new ground state $f(y)$) that can be integrated to the leading order in large y_0 to yield

$$l = \int_0^\infty 1 - \tanh(y/\sqrt{2})^2\, dy = \sqrt{2}. \tag{2.16}$$

Therefore, the velocity of the vortex next to the wall is (to the leading order in large y_0)

$$U = 1/(2y_0 - 2\sqrt{2}). \tag{2.17}$$

The generalisation of this result were made [**19**] for inhomogeneous (trapped) condensates. In general, the velocity can be found by using the area of the displaced density at the boundary to determine the shift l in the position of the image vortex.

3. Nonlocal Model

Although the GP equation is a popular model of superfluid helium, several aspects of the local GP model (1.5) are qualitatively or quantitatively unrealistic in application to superfluid helium. Superfluid helium is not a weakly interacting Bose gas, instead it is a strongly correlated fluid dominated by many-body effects. The velocity, c, of long wavelength sound waves is proportional to $\rho^{\frac{1}{2}}$ in the GP equaton, but it is known from helium experiments [**20**] that $c \propto \rho^{2.8}$. Next, the dispersion relation (1.15) does not

describe a characteristic dip (roton minimum) in the superfluid helium dispersion curve. The omission of the roton branch is not too serious at low temperatures, where only the phonon branch is significantly populated, but it may have some repercussions when studying reconnection processes. The last two of these weaknesses are removed by replacing the local model (1.5) by a suitably chosen nonlocal model as in [**21, 22, 23**]. The minimum requirements on such a potential would be (i) the correct position of the roton minimum and (ii) the correct speed of sound. Actually such a fit can be obtained with a variety of potentials. Pomeau and Rica [**21**] pioneered the use of nonlocal models for study superfluidity, but their model did not have the correct sound velocity (slope of the dispersion curve at the origin) of superfluid helium. The applicability of (1.4) with a potential that adequately represents the dispersion curve has been analysed in [**22**]. It was shown that for liquid helium having the correct Landau dispersion curve, solutions of equation (1.4) develop non-physical mass concentrations. In particular, the "Eulerian part" of the momentum equation (without the quantum stress tensor) may become no longer hyperbolic in some parts of the integration volume. A virial theorem, similar to the one used to establish the catastrophic blow-up in the focusing nonlinear Schrödinger equation, can be used to establish similar catastrophes in bounded volume for (1.4). This indicates that the assumptions underlying the derivation of the equation break down and that higher order nonlinearities must be introduced.

A more accurate approach in modelling liquid helium is through density-functional theory done by Dalfovo et al. [**24**], which attempts to give an adequate microscopic description of interactions. In this approach the total energy is still written as a functional of the one-body density, but it includes short-range correlations. This approach has provided a quantitatively and qualitatively reliable representation of the superfluid properties of free surfaces, helium films, and droplets (see [**24**] and references therein). At the same time this approach is phenomenological and results in rather complicated forms of the energy functionals with many parameters that are chosen to reproduce liquid helium properties.

The nonlocal model (1.4) was modified in [**23**] in the spirit of a density - functional approach, by introducing only one additional nonlinear term in the expression for the correlation energy. This remedies the nonphysical features of model (1.4), while retaining not only an adequate representation of the Landau dispersion relation, but also simplicity in the analytical and numerical studies.

The idea is to replace the potential part of (1.8) which we write as $E_{\rm int} = \frac{V_0}{2m^2}\int \rho^2\, d\mathbf{x}$ by

$$E_{\rm int} = \frac{1}{m^2}\int\left[\frac{1}{2}\int \rho(\mathbf{x}')V(\mathbf{r}'-\mathbf{r})\rho(\mathbf{x})\, d\mathbf{x}' + \frac{W}{4\gamma+1}\rho^{4\gamma+1}\right] d\mathbf{x}, \tag{3.1}$$

where W and γ are phenomenological constants. $V(|\mathbf{x}-\mathbf{x}'|)$ is chosen so that the implied dispersion relation is a good fit to the Landau dispersion curve, for instance by considering a potential of the form

$$V(|\mathbf{x}-\mathbf{x}'|) = V(r) = (\alpha + \beta A^2 r^2 + \delta A^4 r^4)\exp(-A^2 r^2). \tag{3.2}$$

where A, B, α, β, and δ are parameters that can be chosen to give excellent agreement with the experimentally determined dispersion curve.

On adopting (3.1), one can see that (1.4) is replaced by

$$i\hbar\psi_t = -\frac{\hbar^2}{2m}\nabla^2\psi + \psi\int |\psi(\mathbf{x}',t)|^2 V(|\mathbf{x}-\mathbf{x}'|)\, d\mathbf{x}' + W\psi|\psi|^{4\gamma} - E_v\psi. \tag{3.3}$$

This model not only produces the structure and energy per unit length of the straight-line vortex that are very close to those obtained from the Monte Carlo simulations by Sadd et al. [**25**], but it also made it possible to bring the vortex core parameter (2.7) and the healing length into agreement. Fig.2 gives the density in the core of the straight line vortex, both for (3.3) and for the GP model. This nonlocal modification of the GP equation has been used to elucidate the differences between roton emission and vortex nucleation [**26**] and to predict what was later identified as a phase transition from a spatially homogeneous state to a layered state characterised by a periodic density modulation [**27**].

FIGURE 2. The amplitude of the vortex line as given by Eq. (3.3) with $\gamma = 2.8$ (solid line), $\gamma = 1$ (short dashed line) and by the GP equation (1.5) (long dashed line).

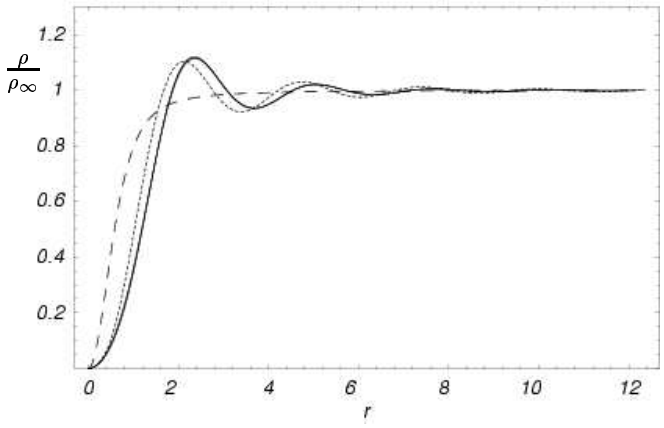

4. Travelling coherent structures in condensates

In this section we address the question of what kinds of travelling waves can exist in superfluid models. In particular we consider three models: the local GP equation (1.5), the nonlocal GP model (3.3) and the system of coupled GP equations that describe two-component BECs.

4.1. Travelling waves in the local GP equation. Firstly, we consider the travelling coherent structures that exist in the local GP equation (1.16). We are interested in localized disturbances moving with constant velocity U in x-direction, so they satisfy

$$2iU\frac{\partial\psi}{\partial x} = \nabla^2\psi + (1-|\psi|^2)\psi, \qquad |\psi| \to 1 \quad \text{as} \quad |\mathbf{x}| \to \infty. \tag{4.1}$$

Velocity of sound is given by $c = 1/\sqrt{2}$.

4.1.1. *1D: dark solitons.* Equation (4.1) in 1D with $\nabla^2\psi$ replaced by $d^2\psi/dx^2$ can be integrated exactly [**28**]. We multiply the GP equation (4.1) by ψ^*, subtract c.c, and look for solutions with constant $Im(\psi)$. From compatibility of equations for real and imaginary parts we obtain

$$Im(\psi) = \sqrt{2}U = U/c, \qquad \sqrt{2}\frac{Re(\psi)}{dz} = \left(1 - \frac{U^2}{c^2} - Re(\psi)^2\right). \tag{4.2}$$

The solutions are found by integrating the second of Eqs. (4.2) and using the boundary conditions. Dark soliton (in dimensional units) has form

$$\psi(x-Ut) = \sqrt{\frac{\rho_\infty}{m}}\left(i\frac{U}{c} + \sqrt{1-\frac{U^2}{c^2}}\tanh\left[\frac{x-Ut}{\sqrt{2}a}\sqrt{1-\frac{U^2}{c^2}}\right]\right). \tag{4.3}$$

Figure (3) shows the graphs of the solitons for various U. Note that the minimum of the density is at $\rho(0) = \rho_\infty U^2/c^2$, so that for $U = 0$, $\psi = 0$. This dark soliton is often referred to as black soliton and the solitons with $U \neq 0$ are gray solitons. The width of the solutions is $\sqrt{2}a/\sqrt{1-U^2/c^2}$ and the phase of the wavefunction experiences a jump $\Delta S = 2\arccos(U/c)$ between $-\infty$ and $+\infty$. Finally, as $U \to c$, the energy E decreases: therefore, the dissipative effects result in an acceleration of soliton and its disappearance.

FIGURE 3. The density of dark solitons for various U as given by Eq. (4.3). The distance is in healing lengths.

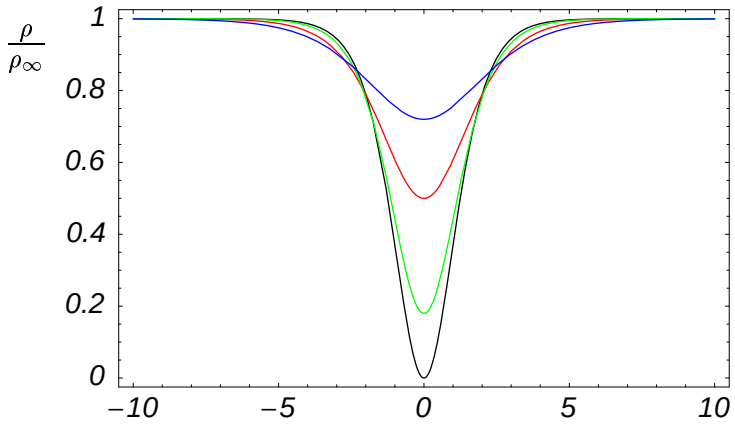

4.1.2. *2D and 3D: vortex pairs, vortex ring and rarefaction waves.* Large vortex rings and vortex pairs were investigated in [**29**] where the following expressions for the energy per unit length, momentum, and velocity, v, were obtained:

$$E = \tfrac{1}{2}\rho\kappa^2 R\left(\ln\frac{8R}{a} + L_0 - 2\right), \quad p = \rho\kappa\pi R^2, \tag{4.4}$$

$$v = (\kappa/4\pi R)\left(\ln\frac{8R}{a} + L_0 - 1\right). \tag{4.5}$$

As expected, $E \approx 2\pi R E_\ell$, but also rings obey Hamilton group relation

$$v = \partial E/\partial p. \tag{4.6}$$

Jones and Roberts [**18**] determined the entire sequence of vortex rings numerically for the GP model (1.16). They calculated the energy E and momentum p and found two branches meeting at a cusp where p and E assume their minimum values, p_m and E_m. As $p \to \infty$ on each branch, $E \to \infty$. On the lower branch the solutions are asymptotic to the large vortex rings (4.4)-(4.5).

As E and p decrease from infinity along the lower branch, the solutions begin to lose their similarity to large vortex rings, and (4.4) - (4.5) determine E, p, and v less and less accurately, although (4.6) still holds. Eventually, for a momentum p_0 slightly greater than p_m, the rings lose their vorticity (ψ loses its zero), and thereafter (for $U > 0.625$) the solitary solutions may better be described as 'rarefaction waves'. The upper branch consists entirely of these and, as $p \to \infty$ on this branch, the solutions asymptotically approach the rational soliton solution of the Kadomtsev-Petviashvili (KP) equation and are unstable. The pE dispersion curve of the solutions in 3D is shown on Fig. (4)(a). The stability of 2D and 3D solutions was analysed in [**30**]. The lower branch is linearly stable and the upper branch is linearly unstable to axisymmetric infinitesimal perturbations, but the growth rates are small.

In two-dimensions, there is only one branch of the solutions that terminates at $p = 0$ and $E = 0$. Large p and E correspond to vortex pairs of opposite circulation. As both p and E decrease the velocity increases, the distance between vortices decreases until at some non-zero p and E the zeros of ψ coincide and for even smaller values of p and E the solutions become rarefaction pulses. Figure 4(b) shows the pE dispersion curve in 2D. The solutions in 2D are linearly stable [**30**].

FIGURE 4. Energy E as a function of momentum p for three-dimensional (a) and two-dimensional (b) travelling coherent solutions of the GP equation (1.16). Rarefaction pulses are shown as dark (red) lines, vortex rings (pairs) are shown as light (green) lines.

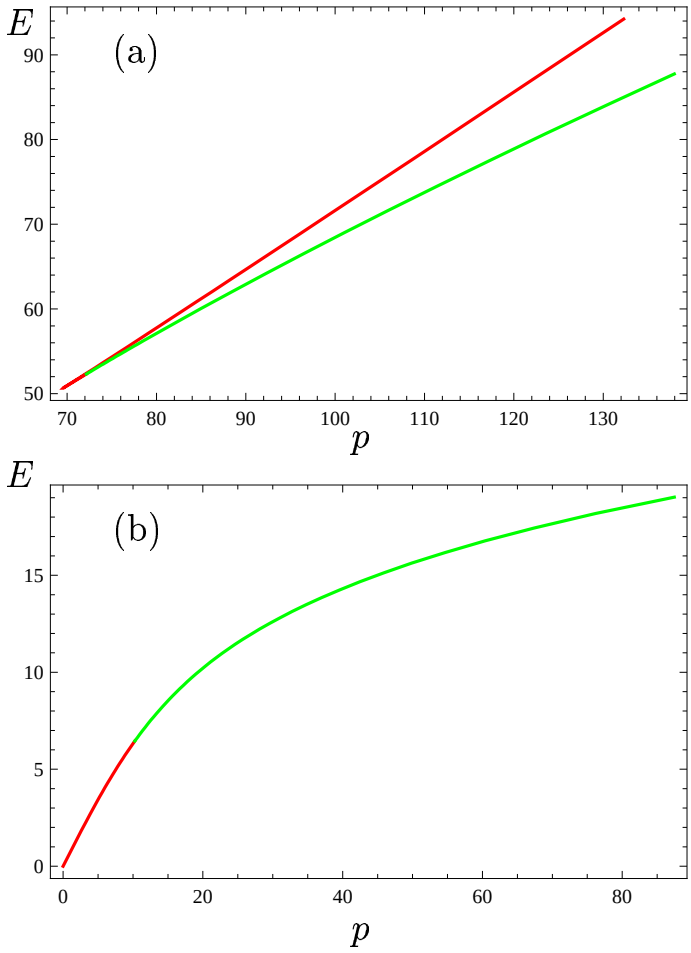

4.2. Travelling waves in the nonlocal GP model. Equation (3.3) was integrated numerically in [**23**] to elucidate the behaviour of vortex rings. These calculations indicate that when the velocity of the vortex ring reaches the Landau critical velocity the ring becomes unstable and evanesces into sound waves. For any ring travelling with speed greater than the Landau critical velocity, the amplitude of the far-field solution will not decay exponentially at infinity, which makes the existence of such a ring impossible. One of the goals of these calculations was to clarify Onsager's concept of the roton as "the ghost of a vanished vortex ring." One can hope that the transition from the vortex ring to the sound pulse and the concomitant loss of vorticity would occur close to the roton minimum in energy-momentum space, or (more probable) close to the point where the group velocity and the phase velocity are equal (the Landau critical velocity u_L). Their calculations show that indeed there is a point on the $pE-$ plane where the ring ceases to exist and where $u_L = \partial E/\partial p$, but this point lies far from the roton minimum, see Fig. 5). It remains to be seen whether the idea of the roton as a ghostly vortex ring will

FIGURE 5. The dispersion relation pE of superfluid helium (dots) and a family of the vortex rings as solutions of Eq. (3.3) (solid lines).

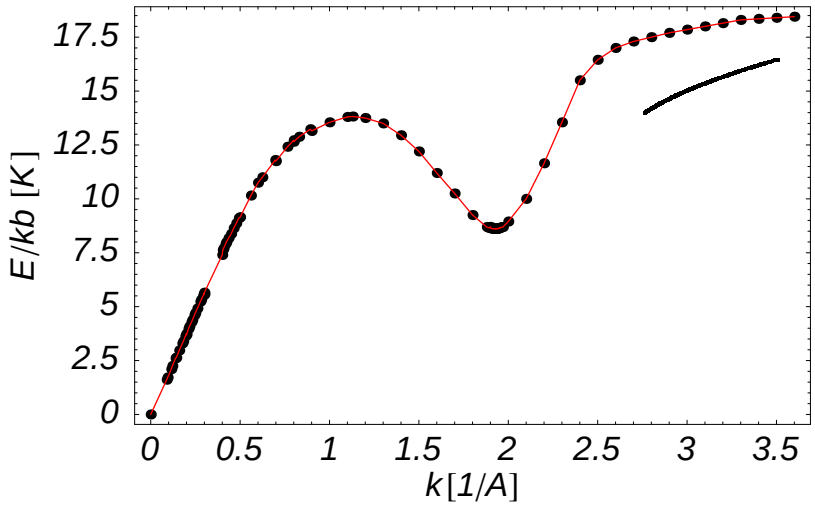

ever be vindicated. As one has a great variety of potentials that lead to the Landau dispersion curve one can tune the parameters so that the line $E = u_L p$, meets the $pE-$ curve for the family of the vortex rings, to allow this sequence of vortex rings to be terminated at a lower energy and momentum level. Whether this process will lead to coalescence with the roton minimum is not yet clear.

4.3. Travelling waves in the coupled Gross-Pitaevskii system. The simplest example of a multi-component system is a mixture of two different species of bosons, for instance, ^{41}K-^{87}Rb [**31**]. Since alkali atoms have spin, it is also possible to make mixtures of the same isotope, but in different internal spin states, for instance, for ^{87}Rb [**32**]. The multi-component BECs are far from being a trivial extension of a one-component BEC and present novel and fundamentally different scenarios for their excitations and ground state. For two components, described by the wave functions ψ_1 and ψ_2, with N_1 and N_2 particles respectively, the GP equations become

$$\begin{aligned} i\hbar\frac{\partial\psi_1}{\partial t} &= \left[-\frac{\hbar^2}{2m_1}\nabla^2 + V_{11}|\psi_1|^2 + V_{12}|\psi_2|^2\right]\psi_1, \\ i\hbar\frac{\partial\psi_2}{\partial t} &= \left[-\frac{\hbar^2}{2m_2}\nabla^2 + V_{12}|\psi_1|^2 + V_{22}|\psi_2|^2\right]\psi_2, \end{aligned} \tag{4.7}$$

where m_i is the mass of the atom of the ith condensate, and the coupling constants V_{ij} are proportional to scattering lengths a_{ij} via $V_{ij} = 2\pi\hbar^2 a_{ij}/m_{ij}$, where $m_{ij} = m_i m_j/(m_i + m_j)$ is the reduced mass. The energy functional of the system (e.g. [**33**]) is

$$E = \int\left[\sum_{i=1}^{2}\{\frac{\hbar^2}{2m_i}|\nabla\psi_i|^2 + \frac{1}{2}V_{ii}|\psi_i|^4\} + |\psi_1|^2 V_{12}|\psi_2|^2\right] d\mathbf{x}. \tag{4.8}$$

In this section we study the solitary wave solutions of the coupled GP model (4.7). Many solitary wave structures have been recently identified in two-component one-dimensional BECs [**34**] such as bound dark-dark, dark-bright, dark-antidark, dark-grey, etc. complexes. In higher dimensions, domain walls [**35**] and skyrmions (vortons) [**36**] have been found. To study the equilibrium properties the energy

functional (4.8) has to be minimized subject to the constraints on the conservation of particles leading to introduction of two chemical potentials $\mu_1 = V_{11}n_1 + V_{12}n_2, \mu_2 = V_{12}n_1 + V_{22}n_2$, where $n_i = |\psi_i|^2$ is the number density in equilibrium. The dispersion relation between the frequency ω and the wave number k of the linear perturbations ($\propto \exp[i\mathbf{k}\cdot\mathbf{x} - i\omega t]$) around homogeneous states is obtained as

$$(\omega^2 - \omega_1^2)(\omega^2 - \omega_2^2) = \omega_{12}^4, \tag{4.9}$$

where $\omega_i^2(k) = c_i^2k^2 + \hbar^2k^4/4m_i^2$ coincides with a one-component Bogoliubov spectrum with the customary defined sound velocity $c_i^2 = n_iV_{ii}/m_i$ and $\omega_{12}^2 = c_{12}^2k^2$ where $c_{12}^2 = n_1n_2V_{12}^2/m_1m_2$. The system is dynamically stable if the spectrum (4.9) is real and positive which implies that $V_{11}V_{22} > V_{12}^2, V_{ii} > 0$ for stability [**33**]. The acoustic branches of Eq. (4.9) are $\omega_\pm \approx c_\pm k$ with the corresponding sound velocities

$$2c_\pm^2 = c_1^2 + c_2^2 \pm \sqrt{(c_1^2 - c_2^2)^2 + 4c_{12}^4}. \tag{4.10}$$

The solitary waves we seek below are all subsonic, so their velocity U is less than c_-.

A dimensionless form of (4.7) is obtained by introducing the chemical potentials $\psi_i \to \psi_i \exp[-\mathrm{i}\mu_i t/\hbar]$ and using dimensionless units

$$\mathbf{x} \to \frac{\hbar}{(2m_1\mu_1)^{1/2}}\mathbf{x}, \qquad t \to \frac{\hbar}{2\mu_1}t, \qquad \psi_i \to \sqrt{\frac{\mu_1}{V_{11}n_i}}\psi_i. \tag{4.11}$$

This leads to the system of nonlinear Schrödinger equations

$$\begin{aligned} -2i\frac{\partial\psi_1}{\partial t} &= \nabla^2\psi_1 + (1 - |\psi_1|^2 - \alpha_1|\psi_2|^2)\psi_1 \\ -2i\frac{\partial\psi_2}{\partial t} &= \gamma\nabla^2\psi_2 + (1 - \alpha_1|\psi_1|^2 - \frac{\alpha_1}{\alpha_2}|\psi_2|^2 - \Lambda^2)\psi_2, \\ &\psi_1 \to \psi_{1\infty}, \quad \psi_2 \to \psi_{2\infty}, \quad \text{as} \quad |\mathbf{x}| \to \infty, \end{aligned} \tag{4.12}$$

where $\alpha_i = V_{12}/V_{ii}$, $\gamma = m_1/m_2$ and $\Lambda^2 = (\mu_1 - \mu_2)/\mu_1$ is the measure of asymmetry between chemical potentials (where we assume that $\mu_1 > \mu_2$). Note that the use of Feshbach resonances to vary the interactions between atoms makes this entire range of parameters experimentally accessible. The condition of dynamic stability becomes $\alpha_1\alpha_2 < 1$. To also ensure stability against collapse when only the density of one component is varied, the final stability criterion becomes

$$0 < \alpha_1\alpha_2 < 1. \tag{4.13}$$

The acoustic branches (4.10) are

$$c_\pm^2 = \frac{1}{2}\left(\psi_{1\infty}^2 + \frac{\alpha_1}{\alpha_2}\gamma\psi_{2\infty}^2 \pm \sqrt{(\psi_{1\infty}^2 - \frac{\alpha_1}{\alpha_2}\gamma\psi_{2\infty}^2)^2 + 4\alpha_1^2\gamma\psi_{1\infty}^2\psi_{2\infty}^2}\right). \tag{4.14}$$

To find solitary wave solutions moving with velocity U in positive $z-$direction, the following equations were solved [**37**]

$$\begin{aligned} 2\mathrm{i}U\frac{\partial\psi_1}{\partial z} &= \nabla^2\psi_1 + (1 - |\psi_1|^2 - \alpha_1|\psi_2|^2)\psi_1 \\ 2\mathrm{i}U\frac{\partial\psi_2}{\partial z} &= \gamma\nabla^2\psi_2 + (1 - \alpha_1|\psi_1|^2 - \frac{\alpha_1}{\alpha_2}|\psi_2|^2 - \Lambda^2)\psi_2, \\ &\psi_1 \to \psi_{1\infty}, \quad \psi_2 \to \psi_{2\infty}, \quad \text{as} \quad |\mathbf{x}| \to \infty. \end{aligned} \tag{4.15}$$

We are interested in the case when both condensates have nonzero uniform states. The values of the wave-functions of the solitary waves at infinity in (4.12) are given by

$$\psi_{1\infty}^2 = (1 - \alpha_2 + \alpha_2\Lambda^2)/(1 - \alpha_1\alpha_2), \tag{4.16}$$

$$\psi_{2\infty}^2 = \frac{\alpha_2}{\alpha_1}(1 - \alpha_1 - \Lambda^2)/(1 - \alpha_1\alpha_2), \tag{4.17}$$

so that we will assume that

$$\alpha_1 < 1 - \Lambda^2, \qquad \alpha_2 < \frac{1}{1-\Lambda^2}. \tag{4.18}$$

In a compact form the equations (4.15) can be written as

$$2iU\frac{\partial \psi_i}{\partial z} = \frac{m_1}{m_i}\nabla^2\psi_i + f_i(\psi_1,\psi_2)\psi_i, \quad i = 1,2 \tag{4.19}$$

where we used the notation

$$\begin{aligned} f_1(\psi_1,\psi_2) &= 1 - |\psi_1|^2 - \alpha_1|\psi_2|^2, \\ f_2(\psi_1,\psi_2) &= 1 - \alpha_1|\psi_1|^2 - \frac{\alpha_1}{\alpha_2}|\psi_2|^2 - \Lambda^2. \end{aligned} \tag{4.20}$$

Each solitary wave complex that belongs to a family of the solitary wave solutions for a chosen set of $(\alpha_1, \alpha_2, \gamma, \Lambda^2)$ is characterised by its velocity, U, vortex radii b_i, momenta $\mathbf{p}_i = (0, 0, p_i)$, and energy. The impulse of the $i-$th component [**37**] is

$$\mathbf{p}_i = \frac{1}{2i}\int [(\psi_i^* - \psi_{i\infty})\nabla\psi_i - (\psi_i - \psi_{i\infty})\nabla\psi_i^*]\, d\mathbf{x} \tag{4.21}$$

We form the energy, E, by subtracting the energy of an undisturbed system of the same mass for which $\psi_i = const$ everywhere, from the energy of the system with a solitary wave, so that the energy of the system becomes

$$\begin{aligned} E &= \frac{1}{2}\int \{|\nabla\psi_1|^2 + \gamma|\nabla\psi_2|^2 + \frac{1}{2}(\psi_{1\infty}^2 - |\psi_1|^2)^2 \\ &+ \frac{\alpha_1}{2\alpha_2}(\psi_{2\infty}^2 - |\psi_2|^2)^2\}\, d\mathbf{x} + \frac{\alpha_1}{2}\int \prod_{i=1}^{2}(\psi_{i\infty}^2 - |\psi_i|^2)\, d\mathbf{x}. \end{aligned} \tag{4.22}$$

Alternatively, we can write

$$E = \frac{1}{2}\int \sum \left\{ \frac{m_1}{m_i}|\nabla\psi_i|^2 + \frac{1}{2}f_i(\psi_1,\psi_2)(\psi_{i\infty}^2 - |\psi_i|^2) \right\} d\mathbf{x}. \tag{4.23}$$

Several families of solitary wave complexes were found: (1) vortex rings of various radii in each of the components (VR-VR complexes), (2) a vortex ring in one component coupled to a rarefaction solitary wave of the other component (VR-RP and RP-VR complexes), (3) two coupled rarefaction waves (RP-RP complexes), (4) either a vortex ring or a rarefaction pulse coupled to a localised disturbance of a very low momentum (slaved wave) (VR-SW, SW-VR, RP-SW, SW-RP complexes). Fig.6 presents the dispersion curves of three families of the axisymmetric solitary wave solutions for $\gamma = 1$, $\alpha_1 = \alpha_2 = 0.1$ and $\Lambda^2 = 0.1$ and

5. Mechanisms of formation of travelling coherent structures

In the previous section we showed that various modifications of the GP equation have quite different travelling wave sequences. The goal of this section to discuss the ways in which these structures can be formed in superfluids. In spite of differences in the solutions the mechanisms of their formation are quite similar.

FIGURE 6. The dispersion curves of three families of the axisymmetric solitary wave solutions of (4.15) with $\gamma = 1$, $\alpha_1 = \alpha_2 = 0.1$ and $\Lambda^2 = 0.1$. The numbers next to the dots give the velocity of the solitary wave solution. The top (black) branch corresponds to VR-VR (VR-RP for $U = 0.58$) complexes. The middle (green) branch shows p vs E for VR-SW complexes and the bottom (red) branch is the dispersion curve of SW-VR (SW-RP for $U = 0.58$) complexes.

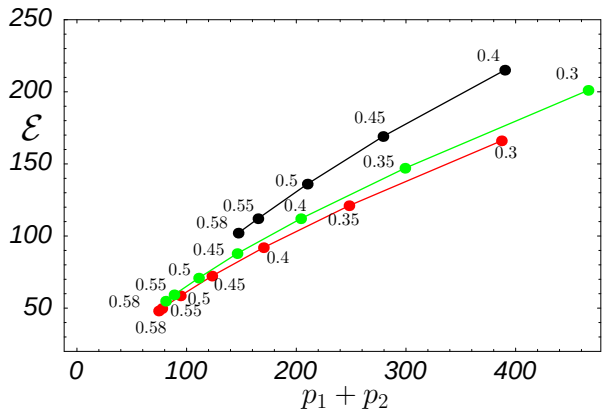

5.1. Critical superflow velocities. Vortex nucleation by an impurity such as the positive ion $^4He_2^+$ moving in superfluid helium at low temperature with velocity v has been studied experimentally and theoretically (see, e.g. [**4**]), and has uncovered some interesting physics. The flow round an ion that is moving with a sufficiently small velocity, v, is well represented by one of the classical solutions of fluid mechanics, namely the flow of an inviscid incompressible fluid around a sphere. In this solution, the maximum flow velocity, $\mathbf{u}$, relative to the sphere is $3v/2$, and occurs on the equator of the sphere (defined with respect to the direction of motion of the sphere as polar axis). Above some critical velocity, v_c, the ideal superflow around the ion breaks down, leading to the creation of a vortex ring. There is some similarity between the flow of the condensate past the ion and the motion of a viscous fluid past a sphere at large Reynolds numbers, the healing layer being the counterpart of the viscous boundary layer. There are, however, important differences. At subcritical velocities, the flow of the condensate is symmetric fore and aft of the direction of motion, and the sphere experiences no drag. In contrast, the viscous boundary layer separates from the sphere, so evading D'Alembert's paradox, destroying the fore and aft symmetry, and therefore bringing about a drag on the sphere. Moreover, when $v > v_c$, shocks form at or near the sphere, but shocks are disallowed in the condensate since they represent a violation of the Landau criterion and a breakdown of superfluidity. When $v > v_c$, the condensate evades shocks through a different mode of boundary layer separation. The sphere sheds circular vortex rings that move more slowly than the sphere and form a vortex street that trails behind it, maintained by vortices that the sphere sheds. As the velocity of the ion increases such a shedding becomes more and more irregular. Each ring is born at one particular latitude within the healing layer on the sphere. As it breaks away into the mainstream, it at first contributes a flow that depresses the mainstream velocity on the sphere below critical. As it moves further downstream however, its influence on the surface flow diminishes. The surface flow increases until it again reaches criticality, when a new ring is nucleated and the whole sequence is repeated. The vortex street trailing behind the ion creates a drag on the ion that decreases as the nearest vortex moves downstream, but which is refreshed when a new vortex is born.

Frisch et al. [**38**] and Winiecki et al. [**39**] have solved numerically the GP equation (1.5) for flow past a circular cylinder and Berloff and Roberts [**40**] for the flow around a positive ion and have confirmed the main features of the scenario just described. Below the critical velocity steady solutions of the GP model exist.

The formation of vortex rings and vortex pairs can be also understood mathematically by considering when the hydrodynamical equations change their type [**41**]. From the Madelung transformations $\psi = R\exp[\mathrm{i}S]$ of the GP equation one gets the following hydrodynamical equations for the number density $n = R^2$ and the phase $\phi = \hbar S/m$ for the superflow with $\phi = u_\infty x$ as $x^2 + y^2 \to \infty$

$$\begin{aligned} &\frac{\partial n}{\partial t} + \nabla \cdot (n \nabla \phi) = 0 \\ &\frac{\partial \phi}{\partial t} + \frac{1}{2}|\nabla \phi|^2 - \frac{1}{2}u_\infty^2 + c^2(\frac{n}{n_\infty} - 1) = c^2 a^2 \frac{\nabla^2 n^{1/2}}{n^{1/2}}. \end{aligned} \tag{5.1}$$

Consider a stationary flow and neglect the quantum pressure term. We fix a point outside of the disk at which the components move with velocities $\mathbf{u}$, introduce the local orthogonal coordinates such that the $x-$axis is tangent to the flow and expand ϕ in the neighbourhood of this point as $\phi \approx ux + \tilde{\phi}$. Linearising for small $\tilde{\phi}$ gives

$$\partial_u (n(u)u)\partial_{xx}\tilde{\phi} + n(u)\partial_{yy}\tilde{\phi} = 0.$$

At low velocities this equation is elliptic and becomes hyperbolic beyond a critical velocity. This happens when $\partial_u(n(u)u) = 0$ on the equator of the disk.

For two-component condensates [**42**] the nucleation condition was obtained in a similar fashion and becomes

$$\frac{\partial(n_1 u_1)}{\partial u_1}\frac{\partial(n_2 u_2)}{\partial u_2} < u_1 u_2 \frac{\partial n_1}{\partial u_2}\frac{\partial n_2}{\partial u_1}. \tag{5.2}$$

Let us consider the motion around a disk in 2D. At subcritical velocity ($U < 0.225$), the flows of the condensates are symmetric fore and aft of the direction of motion, and the disk experiences no drag. When the condition (5.2) is satisfied, which happens first on the disk equator where the velocities are maximal, the condensates evade shocks through a boundary layer separation. Fig. 7 shows the emission of various complexes for the disk of the radius 10 healing lengths that moves with supercritical velocity $U = 0.28$. The disk sheds SW-VP, VP-SW and VP-VP complexes in the order and frequency that depends on the value of the disk's velocity. These complexes move more slowly than the disk and form a vortex wave street that trails behind it, maintained by other complexes that the disk sheds. As the velocity of the disk increases such a shedding becomes more and more irregular. Each complex is born at one particular latitude within the healing layer on the disk. As it breaks away into the mainstream, it at first contributes a flow that depresses the mainstream velocities on the disk below critical. For larger values of the disk velocity ($U > 0.265$), more energy is required for this depression and VP-VP complex that has larger energy than SW-VP complexes is born first. At low supercritical velocities SW-VP complex is born first. As it moves further downstream however, its influence on the surface flow diminishes. The surface flow increases until it again reaches criticality, when a new complex is nucleated and the whole sequence is repeated. The vortex and slaved wave street trailing behind the disk creates a drag on the disk that decreases as the nearest complex moves downstream, but which is refreshed when a new complex is born. The complexes downstream of the disk move with different velocities and interact among themselves. These interactions may lead to a transformation from one type of the complex to another; Fig. 7 shows the splitting of the VP-VP complex into SW-VP and VP-SW complexes. The mechanism in which solitary waves transfer energy from one is discussed in Sec. 5.3 below.

FIGURE 7. The time snapshots of $|\psi_1|^2$ (top) and $|\psi_2|^2$ (bottom) of the solution of Eq. (4.15) with $-2i\psi_{it}$ added to the left hand sides with $\alpha = 0.5$, $\Lambda^2 = 0.1$ for the flow around a disk of radius 10 moving to the right with velocity $U = 0.28$. The solitary wave street is seen in the wake of the disk. The complexes were emitted in the order VP-VP, SW-VP, VP-SW, and SW-VP complex has just got emitted from the disk boundary. For this large supercritical velocity the VP-VP complex is first nucleated from the surface of the disk and the insets show this moment at an earlier time. On the main panels this complex is in the process of splitting into the VP-SW and SW-VP complexes. Only parts of the computational box are shown.

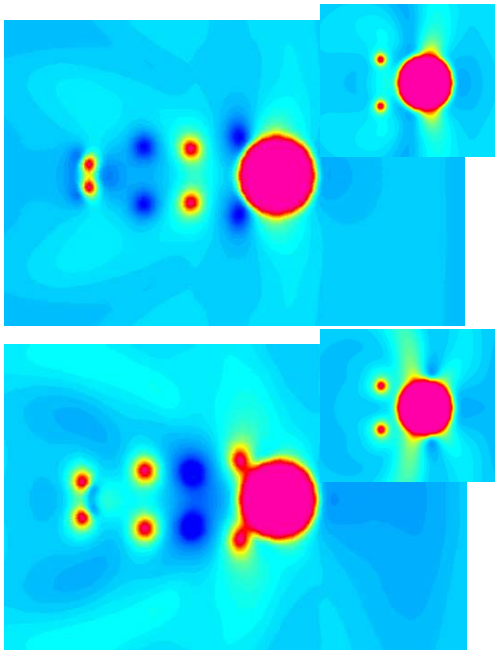

5.2. Transverse "snake" instability. The velocity of dark solitons in the GP equation in 1D depends on the density at the minimum as we previously discussed. This implies [**43**] that if a dark soliton is placed in dimension greater than one it breaks due to transverse perturbation along the front and evolves into vortex ring/pairs or other travelling wave structures.

5.3. Energy transfer. The vortex pairs and vortex rings can appear as a result of an interaction among the solitary wave solutions of the GP equation as was shown in [**14**]. The interactions between various, even vortex-free, solitary waves result in energy and momentum transfer that can lead to vortex nucleation. Rarefaction pulses on the lower branch of the dispersion curve have lower energy and momentum than vortex rings, therefore, such rarefaction pulse may evolve into a vortex ring if interactions with other solutions add enough energy and momentum to the rarefaction pulse. This is illustrated by placing two rarefaction pulses a distance $10a$ apart that move in the same direction. The effect two solitary waves have on each other is non-symmetric. As a result, the rarefaction pulse moving behind transfers part of its energy and momentum to the pulse moving at front, so that the latter transforms into a vortex ring and slows down, whereas the former spreads out and speeds up. This process leads to an even closer interaction of the two solitary waves and an even more rapid transfer

of energy from the solitary wave that moves behind to the one moving at front. Eventually almost all of the energy and momentum of the former is transferred to the latter, which becomes a vortex ring of energy and momentum that are only slightly less than twice the energy and momentum of each of the initial rarefaction pulses. The remaining small energy is emitted as sound waves. Figure 7 gives the graphical illustration of this process through the snapshots of the density cross-sections.

FIGURE 8. The snapshots of the contour plots of the density cross-section of a condensate obtained by numerically integrating the GP model (1.16). Initial condition consists of two rarefaction pulses on the lower branch of the *Ep* cusp. Black solid lines show zeros of real and imaginary parts of ψ, therefore, their intersection shows the position of topological zeros. Both low and high density regions are shown in darker shades to emphasise intermediate density regions. Only a portion of an actual computational box is shown.

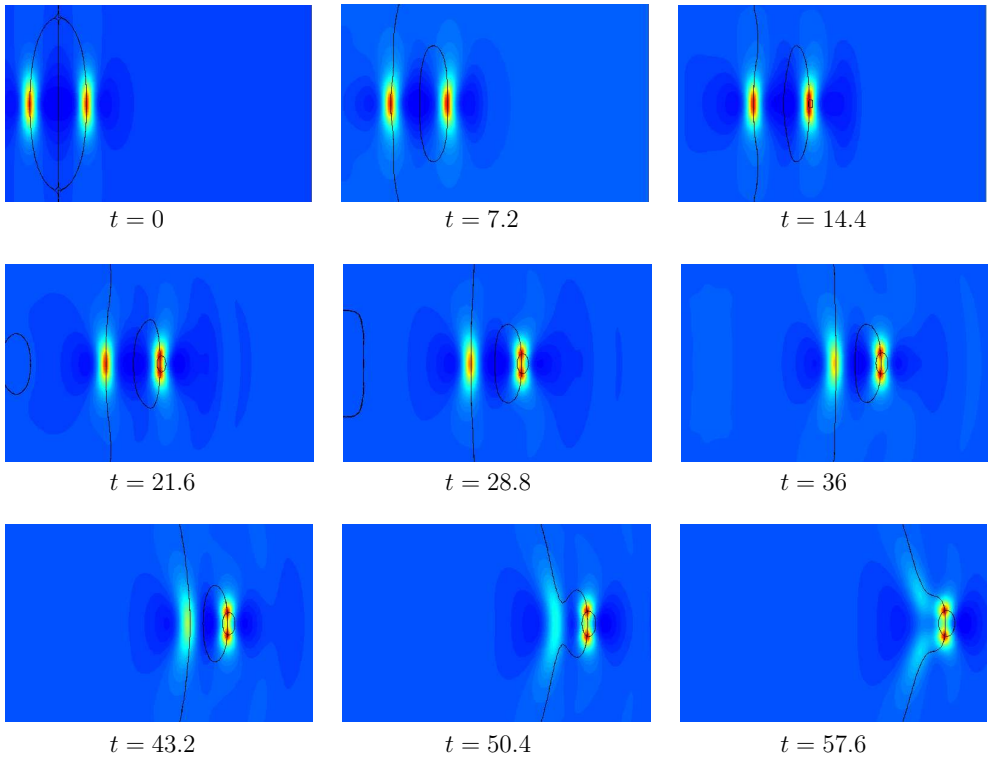

5.4. Collapsing ultrasound bubbles. Experiments in superfluid helium have demonstrated the production of quantised vortices and turbulence [**44**] by the collapse of cavitated bubbles [**45**] generated by ultrasound in the megahertz frequency range.

The time-dependent evolution of the condensate during and after collapse of the bubble involves several stages that were studied in [**46**]. During the first stage dispersive and nonlinear wave trains are generated at the surface of the collapsed bubble. The Fourier components propagate at different velocities generating wave packets moving in opposite directions. This stage of the evolution is characterised by a flux of particles towards the centre of the cavity, while oscillations of growing amplitude are being formed on the real and imaginary parts of the wave function and the slope of the steep density

FIGURE 9. Time snapshots of the density isoplots $\rho = 0.2$ after the collapse of the bubble of radius $a = 50$ centred at the origin. The density plots of the cross-section of the solution at $z = 0, x \in [0, 150], y \in [-25, 25]$ are given at the bottom of each isoplot to indicate the details of the vortex formation. Black solid and dashed lines show zeros of real and imaginary parts of ψ correspondingly, therefore, their intersection shows the position of topological zeros. Both low and high density regions are shown in darker shades to emphasise intermediate density regions. The side of the computational box is 300 healing lengths and the distance between ticks on the side corresponds to 30 healing lengths. The vortex rings nucleate at about $t \sim 50$.

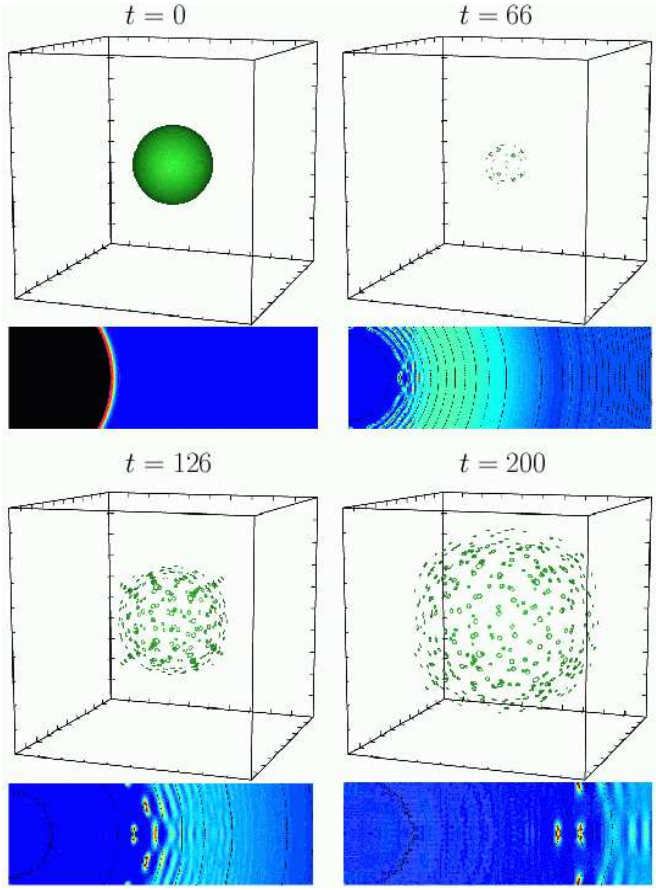

front is getting smaller. There is a moment of time when the density at the centre of what used to be a cavity reaches the maximum value. This moment indicates the start of a qualitatively new stage of the evolution in which there is an outward flux of particles as the condensate that overfilled the cavity begins to expand. The radial density depletions propagate away from the centre and this is when an instability sets in leading to formation of vortex rings and rarefaction pulses, as Fig. 9 illustrates. Note the growth of the vortex rings as they move away from the centre. This is due to the mechanism of energy transfer that we discussed in the previous section.

FIGURE 10. Evolution of topological defects in the phase of the long-wavelength part of the field ψ in the computational box 128^3.

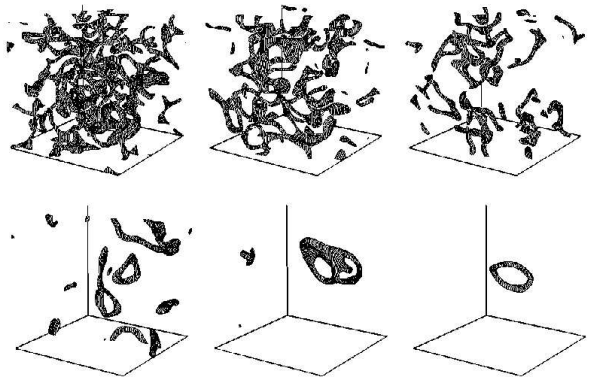

5.5. BEC formation. Finally, the localized disturbances, vortex rings, rarefaction pulses are formed during the BEC formation from a strongly degenerate gas of weakly interacting bosons. As this topic bring us immediately to the discussion of superfluid turbulence we shall discuss the BEC formation in some detail in the next section.

6. Superfluid turbulence in the GP equation

An important and often overlooked feature of the GP equation is that it gives an accurate microscopic description of the formation of BEC from the strongly degenerate gas of weakly interacting bosons [**47, 48**]. In terms of the coherent-state formalism, it was demonstrated that if the occupation numbers are large and somewhat uncertain, then the system evolves as an ensemble of classical fields with corresponding classical-field action leading, in our case to the GP equation. It is important to emphasise that in the context of the strongly non-equilibrium BEC formation kinetics the condition of large occupation numbers is self-consistent: the evolution leads to an explosive increase of occupation numbers in the low-energy region of wavenumber space [**49**] where the ordering process takes place. Even if the occupation numbers are of order unity in the initial state, so that the classical matter field description is not yet applicable, the evolution that can be described at this stage by the standard Boltzmann quantum kinetic equation inevitably results in the appearance of large occupation numbers in the low-energy region of the particle distribution. The blow-up scenario [**49**] indicates that only low-energy part of the field is initially involved in the process. Therefore, one can switch from the kinetic equation to the matter field description for the long-wavelength component of the field at a certain moment in the evolution when the occupation numbers become appropriately large.

The formation of the large-scale coherent localized ground state (condensate) from a non-equilibrium initial state has been studied in a number of papers addressing different stages of the formation: weak turbulence [**50, 49**], strong turbulence in the long-wavelength region of energy space [**51**], and finally, the formation of a genuine condensate [**52, 53**]. The superfluid turbulence and evolution of vortex tangle has been extensively studied in [**54, 55**]. The related question about the effect of finite temperature on the BEC dynamics has also been addressed recently [**56**].

Unambiguous demonstration of the formation of the state of superfluid turbulence in the course of self-evolution of weakly interacting Bose gas was performed in [**51**]. The formation of a tangle of well-separated vortices and the decay of superfluid turbulence as well as the formation of a vortex ring are clearly seen on Fig. 10.

When the turbulent tangle of vortices decays the system reaches a state of thermodynamical equilibrium. Number of particles in condensate depends on the total number density $\rho = N/V$ and the energy density of the system These relations were found in [**53**] by adapting the Bogoliubov theory of a weakly interacting Bose gas [**57**] to the classical nonlinear Schrödinger equation

$$i\partial_t\psi = -\nabla^2\psi + |\psi|^2\psi. \tag{6.1}$$

The dynamics conserves the total number of particles $N = \int |\psi|^2 d\mathbf{x}$, and the total energy $E = \int \left(|\nabla\psi|^2 + \frac{1}{2}|\psi|^4\right) d\mathbf{x}$. In terms of the Fourier amplitudes $a_{\mathbf{k}}(t) = \int \psi(\mathbf{x},t)e^{-i\mathbf{k}\cdot\mathbf{x}}\, d\mathbf{x}$ the total energy is written as

$$E = \sum_k k^2 a^*_{\mathbf{k}} a_{\mathbf{k}} + \frac{V_0}{2V}\sum_{1234} a^*_{\mathbf{k}_1} a^*_{\mathbf{k}_2} a_{\mathbf{k}_3} a_{\mathbf{k}_4} \delta_{\mathbf{k}_1+\mathbf{k}_2-\mathbf{k}_3-\mathbf{k}_4}. \tag{6.2}$$

The Bogoliubov transformation [**57**]

$$\begin{pmatrix} a_{\mathbf{k}} \\ a^*_{-\mathbf{k}} \end{pmatrix} = \begin{pmatrix} u_+ & u_- \\ u_- & u_+ \end{pmatrix} \begin{pmatrix} b_{\mathbf{k}} \\ b^*_{-\mathbf{k}} \end{pmatrix}, \qquad u_\pm = (1 \pm \Gamma_k^2)/2\Gamma_k, \qquad \Gamma_k = \sqrt{\frac{k^2}{\omega(k)}}$$

is used to diagonalise the quadratic (in $k \neq 0$) term to

$$\sum_{k\neq 0} \omega(k) b^*_{\mathbf{k}} b_{\mathbf{k}}, \qquad \omega(k) = \sqrt{k^4 + 2V_0\rho_0 k^2}, \qquad \rho_0 = n_0/V,$$

where $\omega(k)$ is the Bogoliubov dispersion relation that takes into account nonlinear interactions and $n_0 \equiv |a_0|^2$ is the number of particles in condensate. The particle number density is

$$\rho = N/V = \sum_{\mathbf{k}} \langle a^*_{\mathbf{k}} a_{\mathbf{k}}\rangle = \rho_0 + \sum_{k\neq 0} (u_+^2 + u_-^2)\langle b^*_{\mathbf{k}} b_{\mathbf{k}}\rangle.$$

The equilibrium distribution of non-condensed particles is found from the kinetic equation modified by the presence of condensate: $n_k^{\rm eq} = T/\omega(k)$ where T is a temperature. In the new basis, the uncondensed mass and energy density become

$$\rho - \rho_0 = \frac{T}{V}\sum_{k\neq 0} \frac{k^2 + V_0\rho_0}{\omega(k)^2}.$$

$$\frac{E}{V} = \frac{1}{2}V_0\left[\rho^2 + (\rho-\rho_0)^2\right] + \frac{T}{V}\sum_{k\neq 0} 1.$$

T/V can be eliminated to yield the expression for the density of the condensed particles as function of the energy density for given total number density.

In Sec.1 we discussed that the vortex lines create a force of mutual friction between superfluid and normal fluid in addition to the mutual friction included by Landau in his equations. We can use the GP equations to represents the effects of collisions of the quasiparticles with the vortex cores. In particular, the vortex line decay law at non-zero temperature was found in [**58**] in the context of the defocusing NLS equation by inserting a vortex ring into a state of thermal equilibrium and following its decay due to the interactions with the non-condensed particles. The result agrees with predictions of the HVBK theory for superfluid helium [**5**] according to which the fundamental equation of the motion of a vortex line, $\mathbf{v_L}$, is given by (see also page 90, Eq. (3.17) of [**4**])

$$\mathbf{v_L} = \mathbf{v_{sl}} + \alpha\mathbf{s}' \times (\mathbf{v_n} - \mathbf{v_{sl}}) - \alpha'\mathbf{s}' \times [\mathbf{s}' \times (\mathbf{v_n} - \mathbf{v_{sl}})], \tag{6.3}$$

where $\mathbf{v_{sl}}$ is the local superfluid velocity that consists of the ambient superfluid flow velocity and the self-induced vortex velocity $\mathbf{u_i}$, $\mathbf{v_n}$ is the normal fluid velocity, $\mathbf{s}$ is a position vector of a point on the vortex and $\mathbf{s}'$ is the unit tangent at that point. Mutual friction parameters α and α' are *ad hoc* coefficients in

FIGURE 11. The proportion of condensed particles to the total number of particles in the system as a function of the energy density for various total number densities.

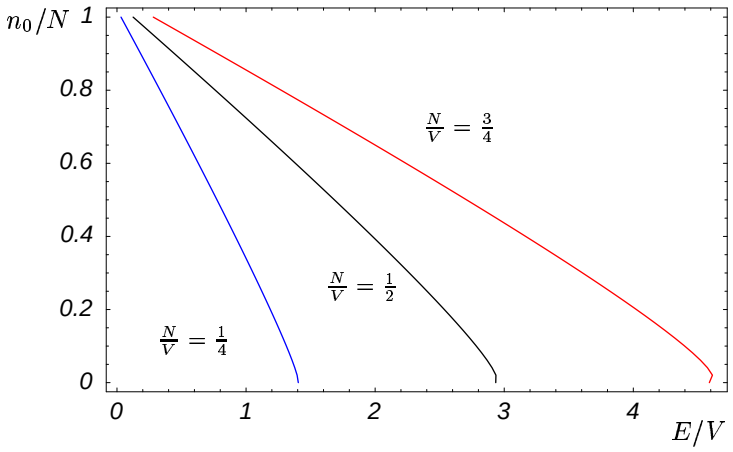

the HVBK theory that are functions of ρ_n, ρ, and T only and but are determined numerically from the GP equation as $\alpha \sim \rho_n T/\rho_s T_\lambda$ and $\alpha' \approx 0$.

Self-evolution of two Bose gases from a strongly non - equilibrium initial state has been studied in [**59**]. It is shown that the large wavelength part of the fields evolves into coherent structures identified as travelling coherent complexes of the coupled nonlinear Schrödinger equations discussed in Sec. (4.3). The evolution of the system is reminiscent of the Kibble-Zurek scenario [**60**] of a formation of the topological defects when the system is quickly quenched below the point of the second-order transition. This process would correspond to the formation of the cosmological *vortons* and *springs* that are analogous to the vortex ring-slaved wave and vortex ring-vortex ring complexes correspondingly [**37**]. Figure 12 shows the evolution fo the long wavelength part of the field and formation of non-axisymmetric VR-VR complex. Collisions with non-condensed quasiparticles lead to the disssipation of the complex and its complete disappearance as the system reaches thermal equilibrium.

References

[1] L. Landau *J. Phys. USSR*, **5**, 71 (1941).
[2] C.F.Barenghi, D.C. Samuels, G.H. Bauer, R.J. Donnelly: Physics of Fluids **9**, 2631 (1997)
[3] C.F.Barenghi, C.J. Swanson, R.J. Donnelly: J. Low. Temp. Phys.**100**, 385 (1995)
[4] R. J. Donnelly *Quantized Vortices in Helium II.* Cambridge: University Press (1991)
[5] H.E. Hall and W.F.Vinen *Proc. R. Soc. Lond., A***238**, 215 (1956)
[6] I.L. Bekharevich and I. M. Khalatnikov *Sov. Phys., JETP*, **13**, 643 (1961).
[7] R.N. Hills and P.H. Roberts *Archiv. Rat. Mech. & Anal.*, **66**, 43 (1977); *Int. J. Eng. Sci.*, **15**, 305 (1977); *J. Low Temp. Phys.*, **30**, 709 (1978); *J. Phys. C***11**, 4485 (1978).
[8] C.F. Barenghi and C. A. Jones *Phys. Lett., A***122**, 425 (1987); *J. Fluid Mech.*, **197**, 551 (1988).
[9] C.E. Swanson and R.J. Donnelly *J. Low Temp. Phys.*, **67**, 185–193 (1987).
[10] P.G. Saffman: *Vortex Dynamics*, (Cambridge University Press, Cambridge, 1992)
[11] M. Leadbeater M., T. Winiecki, D.C. Samuels, C.F. Barenghi and C. S. Adams *Phys. Rev. Letts.* **86** 1410 (2001); N. G. Berloff *Phys. Rev* A**69** 053601 (2004).
[12] V. L. Ginzburg and L. P. Pitaevskii *Zh. Eksp. Teor. Fiz.* **34**, 1240 (1958) [*Sov. Phys. JETP* **7**, 858 (1958)]; E. P. Gross *Nuovo Cimento* **20**, 454 (1961); L. P. Pitaevskii *Soviet Physics JETP*, **13**, 451 (1961).
[13] L.P.Pitaevskii: Sov. Phys. JETP **13**, 451 (1961)
[14] N.G. Berloff, *J. Phys. A: Math. Gen.* **37**, 1617 (2004).
[15] A.L.Fetter, in *Lectures in Theoretical Physics*, edited by K.T.Mahanthappa and W.E. Brittin (Gordon and Breach, New York, 1969), Vol. XIB, p.351.

FIGURE 12. Evolution of topological defects in the long-wavelength parts $\tilde{\psi}_i$, with $i = 1$ (green, light grey) and $i = 2$ (red, dark grey) of the fields ψ_i in the computational box 128^3. The defects are visualised by isosurfaces $|\tilde{\psi}_i|^2 = 0.04\langle|\tilde{\psi}_i|^2\rangle$. High-frequency spatial waves are suppressed by the factor $\max\{1 - k^2/k_c^2, 0\}$, where the cut-off wave number is chosen according to the phenomenological formula $k_c = 9 - t/1000$.

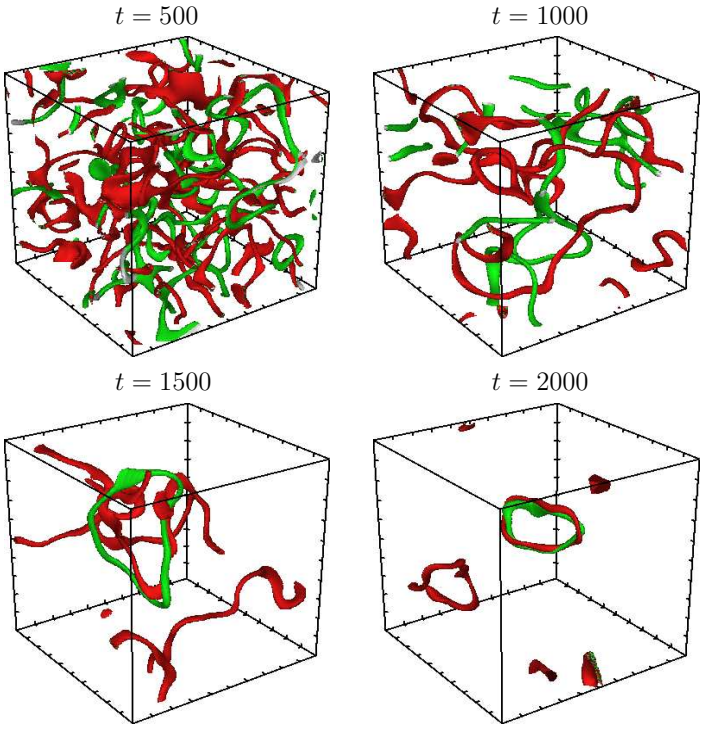

[16] P. H. Roberts, Proc. R. Soc. London A 459, 597 (2003).
[17] P. Mason, N.G. Berloff and A.L.Fetter, *Phys. Rev. A*, **74** , 043611, (2006).
[18] C.A. Jones, P.H. Roberts J. Phys. A: Gen. Phys. **15**, 2599 (1982).
[19] P. Mason and N.G. Berloff *Phys. Rev. A*, **74**, submitted (2007).
[20] J. B. Brooks and R. J. Donnelly *J. Phys. Chem. Ref. Data*, **6**, 51 (1977).
[21] Y. Pomeau, S. Rica Phys. Rev. Lett. **71**, 247 (1993).
[22] N.G. Berloff *J. Low Temp. Phys.*, **116**, 359 (1999).
[23] N.G. Berloff and P.H. Roberts *J. Phys. A***32**, 5611 (1999).
[24] F. Dalfovo, A. Lastri, L. Pricaupenko, S Stringari, J Treiner: Phys. Rev. B **52**, 1193 (1995).
[25] M. Sadd, G.V. Chester, L. Reatto: Phys. Rev. Lett. **79**, 2490 (1997).
[26] N.G. Berloff, P. H. Roberts Phys. Lett. A, **274**, 69-74 (2000).
[27] F. Ancilotto, F. Dalfovo, L. P. Pitaevskii, and F. Toigo *Phys. Rev. B* **71** 104530 (2005).
[28] T. Tsuzuki *J. Low Temp. Phys.* **4** 441 (1971).
[29] P.H. Roberts, J. Grant: J. Phys. A: Gen. Phys. **4**, 55 (1971).
[30] N.G. Berloff and P.H. Roberts, *J. Phys. A:Math. Gen.* **37**, 11333 (2004).
[31] C.J. Myatt *et al.*, *Phys. Rev. Lett.* **78**, 586 (1997); D.S.Hall *et al.*, *Phys. Rev. Lett.* **81**, 1539 (1998); D.M. Stamper-Kurn *et al.*, *Phys. Rev. Lett.* **80**, 2027 (1998) and J. Stenger *et al.*, *Nature* **396**, 345 (1998).
[32] G.Modugno *et al.*, *Phys. Rev. Lett.* **89**, 190404 (2002).
[33] C.J. Pethick and H.Smith, *"Bose-Einstein Condensation in Dilute Gases"*, Cambridge University Press (2002).

[34] P. Öhberg and L. Santos, *Phys. Rev. Lett.* **86**, 2918 (2001); Th. Busch and J.R. Anglin, *Phys. Rev. Lett.* **87**, 010401 (2001) and P.G. Kevrekidis *et al.*, *Eur. Phys. J. D* **28**, 181 (2004).
[35] S. Coen and M. Haelterman, *Phys. Rev. Lett.* **87**, 140401 (2001).
[36] J. Ruostekoski and J.R. Anglin, *Phys. Rev. Lett.* **86**, 3934 (2001); C.M. Savage and J. Ruostekoski, *Phys. Rev. Lett.* **91**, 010403 (2003) and R.A. Battye, N.R. Cooper and P.M. Sutcliffe, *Phys. Rev. Lett.* **88**, 080401 (2002).
[37] N.G. Berloff, *Phys. Rev. Lett.* **94** , 120401 (2005).
[38] T. Frisch, Y. Pomeau, and S. Rica *Phys. Rev. Lett.***69** 1644 (1992).
[39] T. Winiecki, J. F. McCann, C. S. Adams: Phys. Rev. Letts **82**, 5186 (1999).
[40] N.G. Berloff, P. H. Roberts: J. Phys.: Math. Gen. **33**, 4025 (2000).
[41] C. Josserand and Y. Pomeau, *Nonlinearity* **14**, R25-R62 (2001)
[42] N.G.Berloff cond-mat/0412743 (2004).
[43] E. A. Kuznetsov and J. J. Rasmussen *Phys. Rev. E***51** 4479 (1995).
[44] R.F. Carey, J.A. Rooney and C.W. Smith, Physics Letters **65** A, 311 (1978); K.W. Schwarz and C.W. Smith, Physics Letters A **82** 251 (1981).
[45] R.D. Finch, R. Kagiwada, M. Barmatz and I. Rudnick, Phys. Rev. A **134** 1425 (1964).
[46] N.G. Berloff and C.F.Barenghi, *Phys. Rev. Letts.* **93** 090401(2004).
[47] E. Levich and V. Yakhot, J. Phys. A: Math. Gen. **11**, 2237 (1978).
[48] Yu. Kagan and B.V. Svistunov, Phys. Rev. Lett. **79**, 3331 (1997).
[49] B. V. Svistunov *Phys. Rev. B***52**, 3647 (1995).
[50] V.E.Zakharov, S.L. Musher, and A.M.Rubenchik, *Phys. Rep.* **129**, 285 (1985) and S. Dyachenko, A.C. Newell, A. Pushkarev and V.E.Zakharov, *Physica D* **57**, 96 (1992).
[51] N. G. Berloff and B. V. Svistunov, Phys. Rev. A **66**, 013603 (2002)
[52] M.J.Davis, S.A. Morgan, and K. Burnett, *Phys. Rev. Lett* **87**, 160402 (2001) and *Phys. Rev. A* **66**, 053618 (2002)
[53] C. Connaughton *et al*, *Phys. Rev. Lett.* **95**, 263901 (2005).
[54] C. Nore, M. Abid, M. E. Brachet: Phys. Fluids **9**, 2644 (1997)
[55] M.Kobayashi and M.Tsubota, *Phys. Rev. Lett.* **94**, 065302 (2005).
[56] M.Brewczyk et al *J. Phys. B: At. Mol. Opt. Phys.* **40**, R1-R37 (2007) and reference within.
[57] N. N. Bogoliubov, Journal of Physics **11**, 23 (1947).
[58] N.G. Berloff and A.J.Youd, *Phys. Rev. Lett.* **99**, 145301 (2007).
[59] N. G. Berloff and C. Yin, *J. of Low Temp. Phys.*, **145**, 187-207 (2006).
[60] T.W.B. Kibble, *J. Phys. A* **9**, 1387 (1976) and W. H. Zurek, *Nature* **317**, 505 (1985).

Department of Applied Mathematics and Theoretical Physics, University of Cambridge, Cambridge, CB3 0WA, United Kingdom

E-mail address: N.G.Berloff@damtp.cam.ac.uk